

Structural-Spectral Graph Convolution with Evidential Edge Learning for Hyperspectral Image Clustering

Jianhan Qi[✉], Yuheng Jia[✉], Member, IEEE, Hui Liu[✉], Junhui Hou[✉], Senior Member, IEEE

Abstract—Hyperspectral image (HSI) clustering assigns similar pixels to the same class without any annotations, which is an important yet challenging task. For large-scale HSIs, most methods rely on superpixel segmentation and perform superpixel-level clustering based on graph neural networks (GNNs). However, existing GNNs cannot fully exploit the spectral information of the input HSI, and the inaccurate superpixel topological graph may lead to the confusion of different class semantics during information aggregation. To address these challenges, we first propose a structural-spectral graph convolutional operator (SSGCO) tailored for graph-structured HSI superpixels to improve their representation quality through the co-extraction of spatial and spectral features. Second, we propose an evidence-guided adaptive edge learning (EGAEL) module that adaptively predicts and refines edge weights in the superpixel topological graph. We integrate the proposed method into a contrastive learning framework to achieve clustering, where representation learning and clustering are simultaneously conducted. Experiments demonstrate that the proposed method improves clustering accuracy by 2.61%, 6.06%, 4.96% and 3.15% over the best compared methods on four HSI datasets. Our code is available at <https://github.com/jhqi/SSGCO-EGAEL>.

Index Terms—Hyperspectral image, clustering, superpixel, graph neural networks, contrastive learning.

I. INTRODUCTION

HYPERSPECTRAL image (HSI) captures the reflectance of land covers across hundreds of contiguous narrow bands, providing rich and precise spectral information. Classifying the pixels of HSI into different categories is a fundamental task [1], [2], [3], [4], [5], [6], as it describes the spatial distribution of different land covers. This technique is widely applied in various fields, such as precision agriculture [7], environmental monitoring [8], mineral exploration [9], and urban planning [10], [11], [12].

Due to the high cost of obtaining HSI pixel annotations, unsupervised clustering methods that explore the relationships between pixels without labels have gained increasing attention.

Jianhan Qi is with the School of Software Engineering, Southeast University, Nanjing 211189, China (e-mail: qjh@seu.edu.cn).

Yuheng Jia is with the School of Computer Science and Engineering, Southeast University, Nanjing 211189, China, and also with the Key Laboratory of New Generation Artificial Intelligence Technology and Its Interdisciplinary Applications (Southeast University), Ministry of Education, Nanjing 211189, China (e-mail: yhjia@seu.edu.cn).

Hui Liu is with the Department of Computing and Information Sciences, Saint Francis University, Hong Kong (e-mail: h2liu@sfsu.edu.hk).

Junhui Hou is with the Department of Computer Science, City University of Hong Kong, Hong Kong (e-mail: jh.hou@cityu.edu.hk).

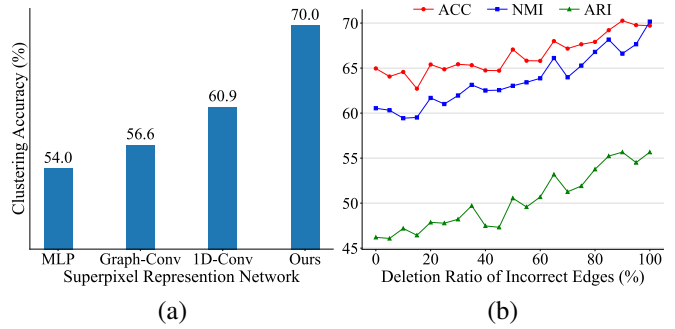


Fig. 1. Motivation of the proposed method: (a) clustering accuracy of different superpixel feature representation networks on *Pavia University* dataset, (b) the impact of deleting incorrect edges on *Pavia University* dataset.

Traditional clustering methods, e.g., K-means [13], fuzzy c-means [14] and subspace clustering [15], [16], have been applied to HSI clustering, but with relatively poor clustering performance. This is because those methods usually perform clustering based on the raw feature of HSI, which is susceptible to spectral noise of HSI caused by the illumination condition or the viewing angle [17]. To this end, research has increasingly turned to deep clustering methods [18], [19], [20], which leverage deep neural networks to learn discriminative feature representations, achieving effective clustering results under end-to-end training. However, the massive number of pixels in HSI may lead to high computational cost. Consequently, many studies employed superpixel segmentation techniques [21], [22], [23] and transformed the clustering task from the pixel level to the superpixel level to reduce the computational cost. Superpixel-level clustering has currently become the mainstream approach for large-scale HSI clustering [24], [25], [26], [27], [28].

Given the irregular shapes and clear spatial distribution, superpixels are naturally modeled as graph-structured data, where each superpixel acts as a node and the topological graph is constructed based on their spatial adjacency or spectral similarity. With the powerful capability of information aggregation, graph neural networks (GNNs) have excelled in graph learning tasks [29], [30], [31]. Consequently, several studies have employed GNNs for superpixel representation learning to incorporate topological information into superpixel embeddings and then conducted GNN-based clustering, which can be mainly categorized into two types. The first

type is based on graph autoencoders (GAEs) [32], which typically reconstruct the graph adjacency matrix from node embeddings, and introduce an auxiliary distribution loss [18] for self-supervised training [33], [34], [35], [36], [37]. The second type utilizes contrastive clustering frameworks [38], [39], [40], conducting alignment or contrast between samples or prototypes to improve the discriminability of superpixel representations [19], [20], [41]. Although the above methods have achieved promising results, **two critical limitations still exist**.

The first limitation concerns insufficient feature extraction from superpixels. Besides the graph structure containing rich spatial information, the spectra of superpixels exhibit continuity and redundancy [42]. While existing GNNs can effectively aggregate spatial information within the neighborhood, the projective transformations (i.e., linear layers) in their networks struggle to capture complex patterns of HSI spectra. Conversely, convolutional neural networks (CNNs) are adept at extracting high-order spectral features, but fail to exploit the superpixel topological information. To illustrate representation learning abilities of different networks, in Fig. 1a, we conducted a comparison among MLP, 1D convolution (1D-Conv), graph convolution (Graph-Conv) and our proposed operator designed to extract both spatial and spectral features, indicating that comprehensive superpixel feature extraction significantly enhances the clustering accuracy.

The second limitation is the inaccurate superpixel topological graph. Typically, the superpixel topological graph is constructed based on either spatial adjacency or spectral similarity. The former connects spatially adjacent superpixels as neighbors [27], [41], while the latter determines neighbors based on spectral similarity [33], [35], [36]. Since the graph is constructed without supervision, both types of graphs inevitably contain incorrect edges that connect two superpixel nodes of different classes. Accordingly, these incorrect edges bring semantically different neighbors, leading to distorted node representations and confused class semantics during GNN aggregation. Fig. 1b illustrates the impact of deleting incorrect edges on clustering results. As the deletion ratio increases, clustering performance gradually improves, highlighting the importance of dealing with incorrect edges in the graph.

Based on the above analyses, we propose a structural-spectral graph convolutional operator (SSGCO) to effectively extract spatial and spectral features for HSI superpixels, and an evidence-guided adaptive edge learning (EGAEL) module to refine the superpixel topological graph. SSGCO performs 1D convolution along the spectral dimension to capture high-order spectral patterns, while simultaneously performing aggregation within the neighborhood to exploit spatial information, which is tailored to HSI superpixel representation learning. Fig. 1a shows that the operator itself yields a notable improvement of 9.1% in clustering accuracy. For EGAEL, we represent each edge by the embeddings of its two endpoint nodes and re-predict the edge weight through a learnable MLP adaptively during training, thereby reducing the weights of incorrect edges. Besides, we propose to use the empirical edge weight computed based on clustering confidence and node similarity as evidence to guide the edge weight prediction.

The superpixel adjacency matrix is then momentum updated with predicted edge weights. Finally, we integrate the proposed SSGCO and EGAEL into a contrastive clustering framework, where pixels randomly sampled from superpixels act as augmented views. Neighborhood alignment and prototype contrast are combined as clustering-oriented training objectives, facilitating a mutual promotion between superpixel representation learning and clustering.

The main contributions of this paper are summarized as follows.

- 1) We propose a novel structural-spectral graph convolutional operator, specifically designed for HSI superpixels, which achieves comprehensive co-extraction of both deep spectral patterns and spatial information.
- 2) We propose an evidence-guided adaptive edge learning module to reduce the weights of incorrect edges, mitigating the impact of the inaccurate superpixel topological graph.
- 3) We integrate our method into the contrastive clustering framework and achieve promising clustering performance. Extensive experiments on four HSI benchmark datasets demonstrate the superiority of our method. In particular, our method achieves an average improvement of 4.20% in clustering accuracy on the four datasets.

The rest of this paper is organized as follows. Section II introduces the adopted data preprocessing approaches, including superpixel segmentation and graph construction in HSIs. Section III presents the proposed method in detail. In Section IV, we provide experimental results and analyses on four HSI datasets. Finally, we conclude this work in Section V.

II. DATA PREPROCESSING

To reduce the computational cost on large HSI, we employ entropy rate superpixel segmentation (ERS) [21] to segment the input HSI \mathcal{H} into M non-overlapped superpixels, where each pixel belongs to exactly one superpixel. Specifically, we perform principal components analysis (PCA) on pixel features and then retain the first principal component to obtain the gray-scale image as the input of ERS.

Then, we apply PCA on raw pixel features again, and retain only d components to further reduce the data dimensionality. Let p_i denotes the i -th pixel, sp_j denotes the j -th superpixel, $\mathbf{x}_i^p \in \mathbb{R}^d$ and $\mathbf{x}_j^{sp} \in \mathbb{R}^d$ are their feature vectors respectively, following:

$$\mathbf{x}_j^{sp} = \frac{1}{|sp_j|} \sum_{p_i \in sp_j} \mathbf{x}_i^p, \quad (1)$$

where $|sp_j|$ denotes the number of pixels in sp_j . For the sake of simplicity, we abbreviate \mathbf{x}_j^{sp} as \mathbf{x}_j . Thus, features vectors of all the superpixels are represented as $\mathbf{X} = [\mathbf{x}_1; \dots; \mathbf{x}_M] \in \mathbb{R}^{M \times d}$, where each row corresponds to a superpixel.

Next, we build the superpixel topological graph based on the spatial adjacency of superpixels. Given two pixels p_m and p_n , where p_m belongs to sp_i and p_n belongs to sp_j , if p_m and p_n are adjacent (i.e., the Manhattan distance between their

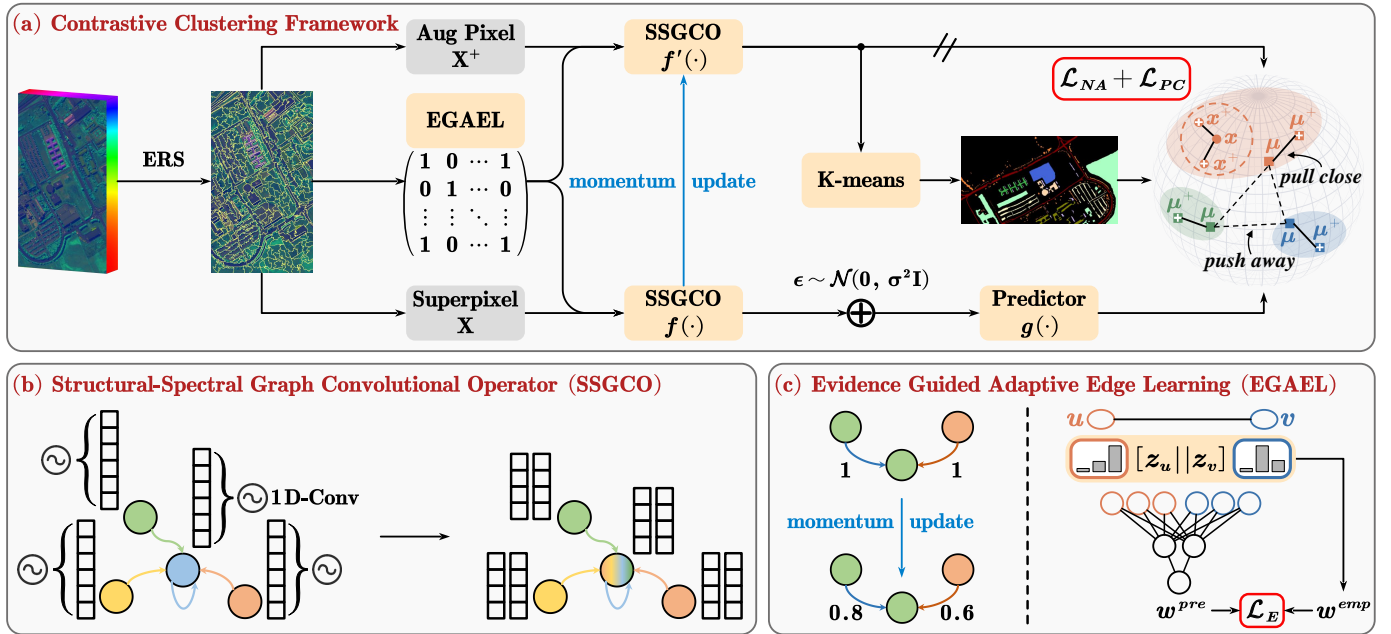


Fig. 2. The diagram of the proposed method: (a) the contrastive clustering framework consists of an online network $f(\cdot)$ and a target network $f'(\cdot)$, which take superpixels and augmented views as inputs. Neighborhood alignment (NA) and prototype contrast (PC) are adopted as training objectives; (b) Structural-spectral graph convolutional operator (SSGCO) simultaneously performs 1D convolution (1D-Conv) and graph convolution in each layer to extract both spatial and spectral features of superpixels; (c) In evidence guided adaptive edge learning (EGAEL), each edge is represented by concatenating the soft assignments of its two endpoint nodes, and input into an MLP to get the predicted edge weight w^{pre} . The empirical edge weight w^{emp} computed with node clustering confidence and similarity is adopted as guidance. The adjacency matrix is momentum updated based on w^{pre} .

coordinates is equal to 1), then sp_i and sp_j are also adjacent. The superpixel adjacency matrix $\mathbf{A} \in \mathbb{R}^{M \times M}$ is defined as:

$$\mathbf{A}_{i,j} = \mathbf{A}_{j,i} = \begin{cases} 1, & \exists p_m \in sp_i, p_n \in sp_j, \text{dis}(p_m, p_n) = 1, \\ 0, & \text{else,} \end{cases} \quad (2)$$

where $\text{dis}(\cdot)$ denotes the Manhattan distance. Following [29], we add self-loop to \mathbf{A} and employ the re-normalization trick:

$$\tilde{\mathbf{A}} = \mathbf{A} + \mathbf{I}_M, \quad (3)$$

$$\tilde{\mathbf{D}}_{i,i} = \sum_j \tilde{\mathbf{A}}_{i,j} \quad (4)$$

$$\hat{\mathbf{A}} = \tilde{\mathbf{D}}^{-\frac{1}{2}} \tilde{\mathbf{A}} \tilde{\mathbf{D}}^{-\frac{1}{2}}, \quad (5)$$

where $\mathbf{I}_M \in \mathbb{R}^{M \times M}$ is the identity matrix, $\tilde{\mathbf{D}}$ is the degree matrix of the adjacency matrix with self-loop, and $\hat{\mathbf{A}}$ is the symmetrically normalized adjacency matrix.

III. PROPOSED METHOD

In this section, we first introduce the adopted contrastive clustering framework, which leverages neighborhood alignment and prototype contrast as training objectives. Second, we introduce the proposed structural-spectral graph convolutional operator, which aims to extract both spatial and spectral features from superpixels. Third, we present the proposed evidence-guided adaptive edge learning to mitigate the impact of incorrect edges in the superpixel topological graph. Finally, we introduce the training procedure in detail. The overall pipeline of our method is illustrated in Fig. 2.

A. Contrastive Clustering Framework

We achieve HSI superpixel clustering under a contrastive clustering framework. Specifically, following [39], [40], we adopt an online network $f(\cdot)$ and a target network $f'(\cdot)$ with identical architecture but unshared parameters as superpixel encoders. To break the symmetry between $f(\cdot)$ and $f'(\cdot)$, and prevent representation collapse, predictor $g(\cdot)$ consisting of two-layer MLP is introduced after $f(\cdot)$. Neighborhood alignment and prototype contrast are combined as clustering-oriented training objectives.

For neighborhood alignment, we first construct reliable positive samples for superpixels through data augmentation. Given superpixel x_i , we randomly select one internal pixel as its augmented view x_i^+ [41]. Then, based on the assumption that representations within a local neighborhood in the embedding space share similar semantics, superpixel representations are encouraged to be similar to not only their augmented views but also neighboring samples, thus improving intra-cluster compactness. Instead of directly sampling from the neighborhood, adopting the reparameterization trick ensures proper gradient back-propagation. For superpixel x_i , its neighborhood in the embedding space can be represented as:

$$v_i = f(x_i) + \sigma \epsilon, \quad (6)$$

where $\epsilon \sim \mathcal{N}(0, \mathbf{I})$ and σ is a hyperparameter that controls the margin of the neighborhood. By minimizing the distance between samples and corresponding augmented views, the

neighborhood alignment is formally defined as:

$$\begin{aligned}\mathcal{L}_{NA} &= \frac{1}{M} \sum_{i=1}^M \|g(\mathbf{v}_i) - f'(\mathbf{x}_i^+)\|_2^2 \\ &= \frac{1}{M} \sum_{i=1}^M \|g(f(\mathbf{x}_i) + \sigma\epsilon) - f'(\mathbf{x}_i^+)\|_2^2.\end{aligned}\quad (7)$$

For prototype contrast, we first perform l_2 -normalization on $f'(\mathbf{x})$ and conduct spherical K-means to obtain a clustering assignment. Let K denote the total number of classes and S_k denotes the set of samples assigned to the k -th cluster, then two views of the k -th prototype, μ_k and μ_k^+ , are defined as the average of sample embeddings in the cluster:

$$\mu_k = \frac{\sum_{x \in S_k} f(\mathbf{x})}{\|\sum_{x \in S_k} f(\mathbf{x})\|_2}, \quad \mu_k^+ = \frac{\sum_{x \in S_k} f'(\mathbf{x}^+)}{\|\sum_{x \in S_k} f'(\mathbf{x}^+)\|_2}. \quad (8)$$

Given one prototype, the remaining $K - 1$ prototypes are definitely negative examples. We construct a contrastive loss [43] to encourage the alignment between different views of the same prototype, and increase the inter-cluster distance, i.e.,

$$\mathcal{L}_{PC} = \frac{1}{K} \sum_{k=1}^K -\log \frac{\exp(\mu_k \cdot \mu_k^+ / \tau)}{\sum_{j=1}^K \exp(\mu_k \cdot \mu_j^+ / \tau)}, \quad (9)$$

where $\tau \in (0, 1)$ is the temperature scaling. With the weight hyperparameter $\alpha > 0$, the total loss for contrastive clustering is defined as:

$$\mathcal{L}_{CC} = \mathcal{L}_{NA} + \alpha \mathcal{L}_{PC}. \quad (10)$$

For optimization, $f(\cdot)$ with parameters θ is updated through gradient back-propagation, while $f'(\cdot)$ with parameters θ' is momentum updated, following:

$$\theta' = m\theta' + (1 - m)\theta, \quad (11)$$

where $m \in (0, 1)$ is the momentum coefficient.

B. Structural-Spectral Graph Convolutional Operator

While existing GNNs excel at leveraging spatial information of HSI based on the superpixel topological graph, they often inadequately extract deep spectral features. Their reliance on projective transformations (i.e., linear layers) limits the capability to deal with the inherent continuity and redundancy of HSI spectra. To address this limitation, we propose a novel structural-spectral graph convolutional operator (SSGCO) to enhance the superpixel representation learning. SSGCO enriches the information aggregation capability of GNNs by infusing dedicated 1D convolutional kernels that target high-order spectral feature extraction, thus simultaneously learning discriminative spectral features and aggregating spatial neighborhood information at the superpixel level.

Based on the standard multi-layer GCN, we additionally introduce 1D convolution along the spectral dimension at each layer to enhance its ability to extract spectral features, as illustrated in Fig. 2b. Then, SSGCO is formally defined as:

$$\mathbf{H}_{(l)} = \phi(\widehat{\mathbf{A}}(\mathbf{H}_{(l-1)} \circledast_{1D} \mathbf{W}_{(l)}^c) \mathbf{W}_{(l)}^g), \quad (12)$$

where $\mathbf{H}_{(l)}$ is the output of the l -th layer and $\mathbf{H}_{(0)} = \mathbf{X}$, \circledast_{1D} denotes 1D convolutional operator, $\mathbf{W}_{(l)}^c$ and $\mathbf{W}_{(l)}^g$ are

TABLE I
STRUCTURAL-SPECTRAL GRAPH CONVOLUTIONAL OPERATOR
FORWARD-PROPAGATION.

Layer	Kernel	Output Dimension
Input	-	(M , 20)
Reshape	-	(M , 1, 20)
1D-Conv	(8, 7)	(M , 8, 14)
BN	-	(M , 8, 14)
Reshape	-	(M , 112)
Graph-Conv	(112, 112)	(M , 112)
BN	-	(M , 112)
Reshape	-	(M , 8, 14)
1D-Conv	(16, 5)	(M , 16, 10)
BN	-	(M , 16, 10)
Reshape	-	(M , 160)
Graph-Conv	(160, 160)	(M , 160)
BN	-	(M , 160)

trainable parameters in the l -th layer corresponding to 1D convolution and graph convolution, $\phi(\cdot)$ is non-linear activation function. Moreover, we conduct batch normalization (BN) [44] after each layer to stabilize the training.

We show a specific example of the proposed SSGCO in Table I, where the input feature dimension d equals to 20 and SSGCO consists of two layers. For 1D convolution (1D-Conv), kernel sizes are set to 7 and 5, numbers of output channels are set to 8 and 16, paddings and strides are set to 0 and 1. For graph convolution (Graph-Conv), we reshape both the input and output representations to keep the dimension alignment. Notably, the kernels of 1D-Conv and Graph-Conv are denoted as (#out channel, #kernel size) and (#in dim, #out dim), respectively.

C. Evidence-guided Adaptive Edge Learning

The superpixel topological graph is usually constructed based on the spatial adjacency. However, incorrect edges that connect superpixels of different classes are harmful to information aggregation in GNNs as they may confuse the semantics of different land covers. To this end, we propose an evidence-guided adaptive edge learning (EGAEL) module to reduce the weights of incorrect edges and improve the quality of the adjacency matrix.

First, we represent each edge by its two endpoint superpixel nodes. Specifically, given an edge $(u, v) \in \mathcal{E}$ where \mathcal{E} denotes the set of all edges in the initial graph, nodes u and v are represented by their soft clustering assignments, i.e., cosine similarity (equals to the dot product since l_2 normalized) between node representations and prototypes:

$$\mathbf{z}_u = [f'(\mathbf{x}_u) \cdot \mu_1, f'(\mathbf{x}_u) \cdot \mu_2, \dots, f'(\mathbf{x}_u) \cdot \mu_K] \in \mathbb{R}^K, \quad (13)$$

$$\mathbf{z}_v = [f'(\mathbf{x}_v) \cdot \mu_1, f'(\mathbf{x}_v) \cdot \mu_2, \dots, f'(\mathbf{x}_v) \cdot \mu_K] \in \mathbb{R}^K, \quad (14)$$

and the feature vector of (u, v) is represented by:

$$\mathbf{z}_{u,v} = [\mathbf{z}_u \parallel \mathbf{z}_v] \in \mathbb{R}^{2K}, \quad (15)$$

where \parallel denotes the concatenating operation. Then, we employ a two-layer MLP $h(\cdot)$ to predict the new edge weight $w_{u,v}^{pre}$:

$$w_{u,v}^{pre} = \varphi(h(\mathbf{z}_{u,v})), \quad (16)$$

where $\varphi(\cdot)$ is the Sigmoid function.

Although $w_{u,v}^{pre}$ can be learned end-to-end under the contrastive clustering loss, the learning process lacks explicit supervision. To this end, we further propose the empirical edge weight as evidence to guide learning. We first define the clustering confidence for node u :

$$\text{conf}_u = \max_{1 \leq k \leq K} f'(\mathbf{x}_u) \cdot \boldsymbol{\mu}_k, \quad (17)$$

and the similarity between nodes u and v :

$$\text{sim}(u, v) = f'(\mathbf{x}_u) \cdot f'(\mathbf{x}_v). \quad (18)$$

Then the empirical edge weight is computed based on a simple intuition: if nodes u and v have higher clustering confidence, higher similarity, and are assigned to the same cluster, then edge (u, v) is more reliable and should be set a higher empirical weight, formulated as:

$$w_{u,v}^{emp} = \varphi((2 \cdot \text{ind}(u, v) - 1) \cdot \text{conf}_u \cdot \text{conf}_v \cdot \text{sim}(u, v)), \quad (19)$$

where $\text{ind}(\cdot)$ indicates whether u and v are assigned to the same class (1 if true, else 0). To constrain the empirical edge weight in $[0, 1]$, we perform min-max normalization on conf_u , conf_v and $\text{sim}(u, v)$ across all edges, and employ the Sigmoid function $\varphi(\cdot)$. Moreover, if u and v are assigned to different classes, we flip the value of $\text{sim}(u, v)$ by setting $\text{sim}(u, v) = 1 - \text{sim}(u, v)$.

Next, we treat the empirical edge weights as prior, and employ mean squared error (MSE) as the loss function to guide the edge learning, encouraging the predicted edge weights $w_{u,v}^{pre}$ to be close to the empirical edge weights $w_{u,v}^{emp}$:

$$\mathcal{L}_E = \frac{1}{|\mathcal{E}|} \sum_{(u,v) \in \mathcal{E}} (w_{u,v}^{pre} - w_{u,v}^{emp})^2. \quad (20)$$

Finally, we build the predicted adjacency matrix \mathbf{A}^{pre} with w^{pre} of all edges, and the original superpixel adjacency matrix is momentum updated to stabilize the training, following:

$$\mathbf{A} = \gamma \mathbf{A} + (1 - \gamma) \mathbf{A}^{pre}, \quad (21)$$

where $\gamma \in (0, 1)$ is the momentum coefficient.

D. Training Procedure

The total loss of the proposed method is defined as the combination of the contrastive clustering loss and the edge learning loss:

$$\mathcal{L} = \mathcal{L}_{CC} + \beta \mathcal{L}_E = \mathcal{L}_{NA} + \alpha \mathcal{L}_{PC} + \beta \mathcal{L}_E, \quad (22)$$

where $\alpha > 0$ and $\beta > 0$ are both weight hyperparameters.

We illustrate the training procedure of the proposed method in algorithm 1. In each epoch, we first compute the empirical edge weights and the predicted edge weights to update the adjacency matrix. Second, we perform forward-propagation, computing node representations, prototypes and loss functions. Third, network parameters are optimized. Fourth, under evaluation mode, we apply spherical K-means on the output of $f'(\cdot)$ to get the current superpixel clustering assignments and then update the prototypes. Finally, we transform the clustering result from the superpixel level to the pixel level by assigning each superpixel's label to its internal pixels.

Algorithm 1 Algorithm of the Proposed Method

Input: Superpixels $\{\mathbf{x}\}$; Adjacency matrix \mathbf{A} ; Online network $f(\cdot)$; Target network $f'(\cdot)$.
Output: Clustering results \mathbf{R} .

- 1: Forward $f'(\mathbf{x})$ by Eq. (12), perform K-means, and compute $\{\boldsymbol{\mu}\}$ by Eq. (8).
- 2: **for** $t = 1$ to T **do**
- 3: Compute $\{w^{emp}\}, \{w^{pre}\}$ by Eqs. (19) and (16), and compute \mathcal{L}_E by Eq. (20).
- 4: Update \mathbf{A} by Eq. (21).
- 5: Randomly sample pixels to get $\{\mathbf{x}^+\}$.
- 6: Forward $f(\mathbf{x}), f'(\mathbf{x}^+)$ by Eq. (12).
- 7: Compute \mathcal{L}_{NA} by Eq. (7).
- 8: Compute $\{\boldsymbol{\mu}\}, \{\boldsymbol{\mu}^+\}$ by Eq. (8).
- 9: Compute \mathcal{L}_{PC} by Eq. (9).
- 10: Compute \mathcal{L} by Eq. (22).
- 11: Update $f(\cdot)$ with SGD optimizer.
- 12: Update $f'(\cdot)$ by Eq. (11).
- 13: Evaluation mode, forward $f'(\mathbf{x})$, perform K-means to get \mathbf{R} , and compute $\{\boldsymbol{\mu}\}$ by Eq. (8).
- 14: **end for**
- 15: Transform \mathbf{R} from the superpixel level to the pixel level.
- 16: **return** \mathbf{R}

TABLE II
OVERVIEW OF *Indian Pines*, *Pavia University*, *Botswana* AND *Trento*.

Dataset	Sensor	Resolution	#Spectral Band	#Class	#Labeled Pixel
<i>Indian Pines</i>	AVIRIS	145 × 145	200	16	10249
<i>Pavia University</i>	ROSIS	610 × 340	103	9	42776
<i>Botswana</i>	Hyperion	1476 × 256	145	14	3248
<i>Trento</i>	AISA Eagle	600 × 166	63	6	30214

IV. EXPERIMENTS

A. Datasets

We evaluated our method on four public HSI datasets, including *Indian Pines*, *Pavia University*, *Botswana* and *Trento*. An overview of all the datasets is shown in Table II.

1) *Indian Pines*: This dataset uses the AVIRIS sensor and has a resolution of 145×145 with 200 spectral bands after removing 24 water absorption bands. It includes 16 different classes with a total of 10249 labeled pixels.

2) *Pavia University*: Utilizing the ROSIS sensor, this dataset has a resolution of 610×340 and 103 spectral bands. It comprises 9 classes and has 42776 labeled pixels.

3) *Botswana*: This dataset is captured with the Hyperion sensor, featuring a high resolution of 1476×256 and 145 spectral bands. It contains 14 classes and a total of 3248 labeled pixels.

4) *Trento*: With the AISA Eagle sensor, this dataset offers a resolution of 600×166 and includes 63 spectral bands. It has 6 classes and 30214 labeled pixels.

B. Experiment Setup

1) *Implementation Details*: The input HSI is standardized across each spectral band. To decrease computational costs, PCA is adopted to reduce the number of bands to 40, 20, 25 and 40 on *Indian Pines*, *Pavia University*, *Botswana* and

TABLE III

CLUSTERING PERFORMANCE ON HSI DATASES. *Indian Pines*, *Pavia University*, *Bo-wana* AND *Trento* ARE ABBREVIATED TO *IP*, *PU*, *BO* AND *TR*, \bullet/\circ INDICATES WHETHER OUR METHOD IS STATISTICALLY SUPERIOR/INFERIOR TO THE COMPARED METHOD ACCORDING TO THE PAIRWISE *t*-TEST AT 0.05 SIGNIFICANCE LEVEL.

Dataset	Metric (%)	K-means [13] (TPAMI 02)	SSC [15] (TPAMI 13)	NCSC [28] (TGRS 22)	SGLSC [27] (TGRS 22)	DGAE [36] (TCSVT 22)	S^3 -ULDA [45] (TGRS 23)	S^2 -DL [46] (TGRS 24)	SDST [35] (TGRS 24)	SPGCC [41] (TCSVT 24)	SAPC [47] (TCSVT 24)	Ours
<i>IP</i>	ACC	34.72 \pm 1.00 \bullet	47.99 \pm 0.46 \bullet	53.48 \pm 0.84 \bullet	58.29 \pm 1.19 \bullet	57.10 \pm 3.39 \bullet	65.41 \pm 3.37 \bullet	64.70 \pm 0.00 \bullet	50.58 \pm 4.46 \bullet	67.40 \pm 1.17 \bullet	55.88 \pm 0.00 \bullet	70.01\pm1.95
	κ	28.39 \pm 1.10 \bullet	42.13 \pm 0.57 \bullet	48.54 \pm 1.12 \bullet	54.54 \pm 1.22 \bullet	52.18 \pm 3.56 \bullet	61.10 \pm 3.50 \bullet	60.24 \pm 0.00 \bullet	44.01 \pm 4.27 \bullet	63.62 \pm 1.34 \bullet	49.59 \pm 0.00 \bullet	66.55\pm2.12
	NMI	43.24 \pm 0.57 \bullet	57.81 \pm 0.44 \bullet	59.47 \pm 1.40 \bullet	63.65 \pm 0.35 \bullet	63.68 \pm 1.03 \bullet	67.65 \pm 1.65 \bullet	71.97\pm0.00	50.21 \pm 1.80 \bullet	67.54 \pm 1.26 \bullet	54.03 \pm 0.00 \bullet	71.17 \pm 1.31
	ARI	21.02 \pm 0.99 \bullet	31.46 \pm 0.55 \bullet	36.13 \pm 1.42 \bullet	40.21 \pm 0.49 \bullet	45.35 \pm 4.75 \bullet	48.99 \pm 3.76 \bullet	52.93 \pm 0.00 \bullet	31.51 \pm 3.83 \bullet	56.02\pm1.94	36.51 \pm 0.00 \bullet	55.99 \pm 2.07
	Precision	37.74 \pm 1.15 \bullet	43.93 \pm 1.72 \bullet	42.74 \pm 2.88 \bullet	51.88 \pm 1.62 \bullet	50.59 \pm 1.81 \bullet	51.34 \pm 1.87 \bullet	59.63\pm0.00	45.34 \pm 2.71 \bullet	52.66 \pm 2.19 \bullet	49.61 \pm 0.00 \bullet	58.72 \pm 2.23
	Recall	40.27 \pm 0.38 \bullet	47.42 \pm 0.56 \bullet	51.12 \pm 0.62 \bullet	57.11 \pm 1.97 \bullet	49.79 \pm 3.89 \bullet	51.11 \pm 3.16 \bullet	59.08 \pm 0.00 \bullet	46.37 \pm 1.38 \bullet	61.34 \pm 3.48 \bullet	52.39 \pm 0.00 \bullet	65.77\pm4.42
	F1	34.24 \pm 0.87 \bullet	40.65 \pm 1.34 \bullet	40.76 \pm 0.92 \bullet	49.50 \pm 1.76 \bullet	46.00 \pm 2.58 \bullet	48.07 \pm 3.10 \bullet	55.19 \pm 0.00 \bullet	44.30 \pm 2.74 \bullet	52.30 \pm 1.89 \bullet	44.67 \pm 0.00 \bullet	57.65\pm2.38
	Purity	52.26 \pm 0.87 \bullet	57.78 \pm 0.51 \bullet	62.87 \pm 0.65 \bullet	69.58 \pm 1.25 \bullet	68.94 \pm 1.51 \bullet	72.52 \pm 2.06 \bullet	75.32\pm0.00	56.51 \pm 1.36 \bullet	73.94 \pm 1.78 \bullet	59.33 \pm 0.00 \bullet	77.18\pm1.03
<i>PU</i>	ACC	51.15 \pm 0.02 \bullet	55.17 \pm 0.00 \bullet	56.08 \pm 3.69 \bullet	57.24 \pm 0.34 \bullet	58.56 \pm 5.21 \bullet	59.42 \pm 0.28 \bullet	60.13 \pm 0.00 \bullet	61.03 \pm 1.80 \bullet	62.62 \pm 0.38 \bullet	63.94 \pm 0.00 \bullet	70.00\pm3.46
	κ	41.49 \pm 0.06 \bullet	45.57 \pm 0.00 \bullet	44.89 \pm 5.06 \bullet	48.28 \pm 0.36 \bullet	49.15 \pm 5.07 \bullet	50.98 \pm 0.47 \bullet	49.06 \pm 0.00 \bullet	50.18 \pm 2.12 \bullet	54.82 \pm 0.46 \bullet	53.02 \pm 0.00 \bullet	62.29\pm3.65
	NMI	53.97 \pm 0.01 \bullet	51.48 \pm 0.00 \bullet	47.34 \pm 4.27 \bullet	53.69 \pm 0.39 \bullet	53.72 \pm 2.58 \bullet	62.93\pm0.08	48.15 \pm 0.00 \bullet	56.41 \pm 1.44 \bullet	57.84 \pm 1.20 \bullet	61.89 \pm 0.00 \bullet	61.90 \pm 3.18
	ARI	31.02 \pm 0.03 \bullet	35.26 \pm 0.05 \bullet	42.84 \pm 5.04 \bullet	42.64 \pm 0.20 \bullet	43.65 \pm 6.69 \bullet	49.04 \pm 0.18 \bullet	43.12 \pm 0.00 \bullet	42.94 \pm 2.63 \bullet	46.19 \pm 0.89 \bullet	44.91 \pm 0.00 \bullet	57.26\pm8.57
	Precision	51.83 \pm 0.01 \bullet	43.00 \pm 0.00 \bullet	40.91 \pm 4.93 \bullet	50.29 \pm 0.39 \bullet	48.16 \pm 4.44 \bullet	56.77\pm0.70	48.68 \pm 0.00 \bullet	53.97 \pm 3.11 \bullet	56.32 \pm 1.16 \bullet	56.21 \pm 0.00 \bullet	57.82\pm1.22
	Recall	53.59 \pm 0.01 \bullet	48.81 \pm 0.00 \bullet	46.19 \pm 7.95 \bullet	53.75 \pm 0.35 \bullet	50.75 \pm 3.47 \bullet	55.63\pm0.51	50.37 \pm 0.00 \bullet	55.34 \pm 1.58 \bullet	58.96 \pm 0.42 \bullet	59.20 \pm 0.00 \bullet	60.55\pm3.09
	F1	50.34 \pm 0.01 \bullet	41.29 \pm 0.00 \bullet	40.09 \pm 5.01 \bullet	48.17 \pm 3.88 \bullet	45.17 \pm 2.27 \bullet	53.21 \pm 0.53 \bullet	40.21 \pm 0.00 \bullet	51.08 \pm 2.06 \bullet	56.05 \pm 0.99 \bullet	56.02 \pm 0.00 \bullet	57.18\pm2.09
	Purity	69.86 \pm 0.00 \bullet	63.87 \pm 0.00 \bullet	64.63 \pm 2.20 \bullet	71.88 \pm 0.20 \bullet	71.17 \pm 1.99 \bullet	76.37 \pm 0.47 \bullet	68.25 \pm 0.00 \bullet	69.80 \pm 1.66 \bullet	77.06\pm0.62	71.32 \pm 0.00 \bullet	77.19\pm2.79
<i>BO</i>	ACC	60.58 \pm 0.13 \bullet	58.54 \pm 1.01 \bullet	47.23 \pm 4.27 \bullet	58.68 \pm 0.01 \bullet	58.48 \pm 1.12 \bullet	45.95 \pm 3.74 \bullet	60.53 \pm 0.00 \bullet	72.70\pm3.18	62.18 \pm 3.45 \bullet	66.10 \pm 0.00 \bullet	77.66\pm1.28
	κ	57.40 \pm 0.15 \bullet	54.93 \pm 1.12 \bullet	42.68 \pm 4.63 \bullet	55.06 \pm 0.01 \bullet	55.09 \pm 1.22 \bullet	41.46 \pm 4.06 \bullet	57.19 \pm 0.00 \bullet	70.40\pm3.48	59.14 \pm 3.73 \bullet	63.17 \pm 0.00 \bullet	75.79\pm1.39
	NMI	69.19 \pm 0.01 \bullet	74.23 \pm 0.10 \bullet	64.14 \pm 1.88 \bullet	67.12 \pm 0.18 \bullet	68.47 \pm 1.34 \bullet	62.40 \pm 2.86 \bullet	68.01 \pm 0.00 \bullet	76.02\pm2.15	73.48 \pm 1.10 \bullet	71.57 \pm 0.00 \bullet	82.90\pm1.30
	ARI	50.08 \pm 0.03 \bullet	52.91 \pm 0.63 \bullet	38.51 \pm 4.18 \bullet	48.08 \pm 0.39 \bullet	44.85 \pm 1.26 \bullet	35.46 \pm 3.93 \bullet	43.76 \pm 0.00 \bullet	58.70\pm3.66	54.06 \pm 2.87 \bullet	48.15 \pm 0.00 \bullet	69.03\pm2.38
	Precision	58.51 \pm 0.07 \bullet	53.43 \pm 1.93 \bullet	43.22 \pm 7.31 \bullet	60.02 \pm 3.43 \bullet	57.02 \pm 1.38 \bullet	41.68 \pm 4.58 \bullet	67.13 \pm 0.00 \bullet	72.81\pm4.06	61.06 \pm 4.54 \bullet	67.66 \pm 0.00 \bullet	73.90\pm2.42
	Recall	62.54 \pm 0.13 \bullet	55.47 \pm 1.56 \bullet	46.23 \pm 3.84 \bullet	55.30 \pm 0.03 \bullet	60.88 \pm 1.24 \bullet	47.71 \pm 3.40 \bullet	60.50 \pm 0.00 \bullet	70.82\pm3.34	61.44 \pm 3.81 \bullet	66.81 \pm 0.00 \bullet	77.65\pm2.39
	F1	58.19 \pm 0.09 \bullet	51.05 \pm 1.77 \bullet	41.29 \pm 4.95 \bullet	53.03 \pm 0.14 \bullet	56.35 \pm 1.36 \bullet	39.24 \pm 3.37 \bullet	60.06 \pm 0.00 \bullet	69.40 \pm 3.12 \bullet	59.04 \pm 4.17 \bullet	64.41 \pm 0.00 \bullet	74.27\pm2.52
	Purity	64.84 \pm 0.12 \bullet	62.03 \pm 0.96 \bullet	50.05 \pm 4.82 \bullet	59.57 \pm 0.01 \bullet	63.77 \pm 1.12 \bullet	48.01 \pm 2.83 \bullet	60.53 \pm 0.00 \bullet	73.31\pm2.33	66.40 \pm 2.20 \bullet	66.10 \pm 0.00 \bullet	77.71\pm1.32
<i>TR</i>	ACC	64.83 \pm 0.02 \bullet	79.18 \pm 0.05 \bullet	75.70 \pm 2.13 \bullet	82.75 \pm 0.27 \bullet	86.50 \pm 0.00 \bullet	75.47 \pm 0.00 \bullet	86.14 \pm 0.00 \bullet	87.97 \pm 0.74 \bullet	89.67 \pm 3.53 \bullet	89.96 \pm 0.00 \bullet	93.11\pm0.96
	κ	55.63 \pm 0.03 \bullet	72.57 \pm 0.07 \bullet	69.00 \pm 2.60 \bullet	77.33 \pm 0.35 \bullet	82.13 \pm 0.00 \bullet	68.62 \pm 0.06 \bullet	81.27 \pm 0.00 \bullet	83.94 \pm 0.91 \bullet	86.38 \pm 4.61 \bullet	86.62 \pm 0.00 \bullet	90.82\pm1.26
	NMI	51.87 \pm 0.01 \bullet	66.73 \pm 0.03 \bullet	72.78 \pm 2.38 \bullet	78.42 \pm 0.06 \bullet	75.62 \pm 0.00 \bullet	77.90 \pm 0.01 \bullet	79.80 \pm 0.00 \bullet	76.15 \pm 1.49 \bullet	85.46 \pm 1.17 \bullet	86.74 \pm 0.00 \bullet	89.74\pm0.94
	ARI	36.82 \pm 0.02 \bullet	55.56 \pm 0.09 \bullet	71.92 \pm 2.15 \bullet	78.27 \pm 0.20 \bullet	79.47 \pm 0.00 \bullet	72.81 \pm 0.00 \bullet	86.44 \pm 0.00 \bullet	82.42 \pm 1.91 \bullet	89.34 \pm 2.26 \bullet	91.69 \pm 0.00 \bullet	94.00\pm1.30
	Precision	59.63 \pm 0.01 \bullet	80.26 \pm 0.02 \bullet	64.54 \pm 4.21 \bullet	63.69 \pm 0.42 \bullet	68.48 \pm 0.00 \bullet	55.46 \pm 0.00 \bullet	68.19 \pm 0.00 \bullet	69.75 \pm 0.72 \bullet	73.89 \pm 7.29 \bullet	84.31 \pm 0.00 \bullet	93.25\pm0.67
	Recall	58.24 \pm 0.01 \bullet	83.02 \pm 0.02 \bullet	60.56 \pm 2.65 \bullet	65.29 \pm 0.32 \bullet	69.84 \pm 0.00 \bullet	59.22 \pm 0.00 \bullet	63.60 \pm 0.00 \bullet	70.15 \pm 0.04 \bullet	76.64 \pm 5.06 \bullet	83.09 \pm 0.00 \bullet	93.11\pm0.96
	F1	55.25 \pm 0.02 \bullet	78.78 \pm 0.03 \bullet	61.57 \pm 3.22 \bullet	60.65 \pm 0.49 \bullet	68.75 \pm 0.00 \bullet	55.81 \pm 0.00 \bullet	62.83 \pm 0.00 \bullet	69.73 \pm 0.44 \bullet	74.31 \pm 6.71 \bullet	82.88 \pm 0.00 \bullet	92.61\pm0.95
	Purity	65.61 \pm 0.01 \bullet	79.18 \pm 0.05 \bullet	87.27 \pm 1.68 \bullet	82.94 \pm 0.27 \bullet	87.09 \pm 0.00 \bullet	86.87 \pm 0.00 \bullet	88.08 \pm 0.00 \bullet	88.66 \pm 0.81 \bullet	91.75 \pm 2.81 \bullet	89.96 \pm 0.00 \bullet	93.66\pm0.74

Trento, respectively. In the contrastive clustering framework, the hidden size of the predictor $g(\cdot)$ is set to 512. The momentum coefficient m for updating $f'(\cdot)$ is set to 0.99. For neighborhood alignment, σ is set to 1×10^{-3} . For prototype contrast, τ is set to 0.7. In the structural-spectral graph convolutional operator, the kernel size of 1D convolution in the first layer is set to 7, with subsequent layers decreasing by 2, but not smaller than 3. The output channels in the first layer is set to 16, with subsequent layers multiplying by 2, but not larger than 64. In the evidence-guided adaptive edge learning, $h(\cdot)$ consists of a two-layer MLP with the hidden size of K . We used the SGD optimizer with the learning rate, weight decay, and momentum coefficient set to 0.05, 5×10^{-4} , and 0.9, respectively. In addition, we adopted cosine annealing and set the learning rate of $g(\cdot)$ 10 \times as that of other modules following [39]. We repeated all experiments five times and reported the mean and standard deviation of the results. We carried out all experiments in a Linux server with an AMD EPYC 7352 CPU and

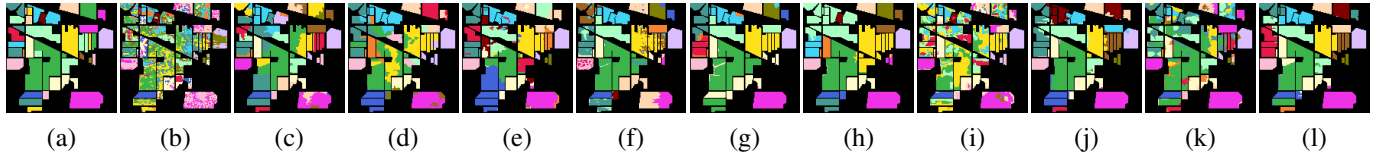


Fig. 3. Clustering maps on *Indian Pines*: (a) ground truth, (b) K-means, (c) SSC, (d) NCSC, (e) SGLSC, (f) DGAE, (g) S^3 -ULDA, (h) S^2 DL, (i) SDST, (j) SPGCC, (k) SAPC, (l) Ours.

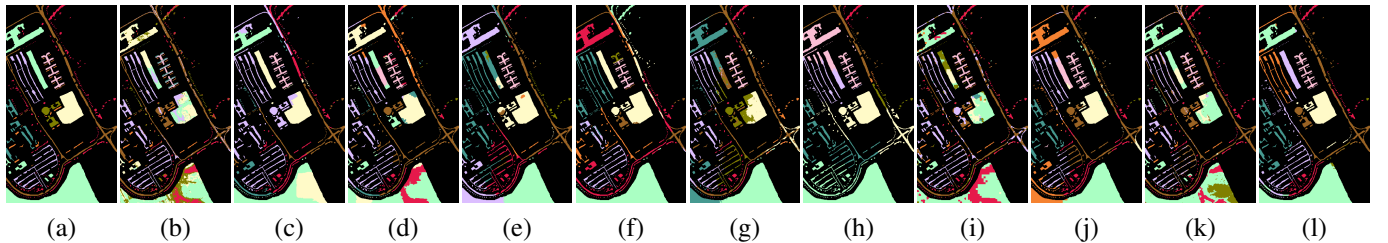


Fig. 4. Clustering maps on *Pavia University*: (a) ground truth, (b) K-means, (c) SSC, (d) NCSC, (e) SGLSC, (f) DGAE, (g) S^3 -ULDA, (h) S^2 DL, (i) SDST, (j) SPGCC, (k) SAPC, (l) Ours.

predicted labels based on the ground truth before calculating clustering metrics.

C. Comparison with State-of-the-Art Methods

We report the clustering performance of our method and other compared methods on *Indian Pines*, *Pavia University*, *Botswana*, and *Trento* in Table III. For each metric, the best value is marked in bold, while the second-best value is underlined.

According to the quantitative clustering metrics, it could be observed that our method outperforms other compared methods with a large margin. For instance, our method improves the ACC by 2.61%, 6.06%, 4.96% and 3.15% on the four datasets. Notably, on *Pavia University*, ACC, K , ARI and F1 obtained by our method outperform the second-best value by 6.06%, 7.47%, 8.22% and 1.13%, respectively. Overall, on *Botswana* and *Trento*, our method achieves the best scores on all metrics; on *Indian Pines*, it achieves the best scores on five metrics and the second-best on three metrics; on *Pavia University*, it achieves the best scores on seven metrics and the second-best on one metric. Based on the results of pairwise t -Test at 0.05 significance level, our method significantly outperforms the compared methods in 91.3% (292/320) of cases.

Compared with subspace-clustering-based methods (i.e., SSC, NCSC and SGLSC) utilizing only spatial information, our method generally brings an improvement of more than 10%. On the basis of the baseline method SSC, SGLSC enhances the similarity between adjacent superpixels by introducing a local superpixel similarity graph. This demonstrates the effectiveness of exploiting spatial information in HSI, which is also the objective behind the use of GCN in our method. Similarly, NCSC achieves the same objective by incorporating neighborhood contrastive regularization. Notably, NCSC leverages 2D convolution to enhance spatial feature extraction at the pixel level. However, the subsequent deep subspace clustering network requires a full batch input, thus incurring substantial memory cost. This limitation motivates us

TABLE IV
RUNNING TIME OF DIFFERENT METHODS (S).

Method	<i>Indian Pines</i>	<i>Pavia University</i>	<i>Botswana</i>	<i>Trento</i>	Avg.
K-means	22.6	113.7	273.9	23.7	108.5
SSC	20.3	16.4	22.3	9.7	17.2
NCSC	77.5	6574.4	8559.3	2900.6	4528.0
SGLSC	108.0	195.6	368.5	173.0	211.3
DGAE	25.5	202.0	12.9	44.4	71.2
S^3 -ULDA	11.5	374.5	2792.4	88.9	816.8
S^2 DL	12.5	544.9	2960.6	65.7	895.9
SDST	296.9	229.7	169.0	129.2	206.2
SPGCC	85.7	619.9	1129.2	437.3	568.0
SAPC	11.1	21.8	51.6	13.2	24.4
Ours	35.0	58.5	51.3	113.0	64.5

to propose the structural-spectral graph convolutional operator that conducts feature extraction entirely at the superpixel level, thereby improving computational efficiency.

Compared with the recent graph contrastive clustering method SPGCC, although both methods employ a similar contrastive clustering framework and superpixel data augmentations, the proposed structural-spectral graph convolutional operator infuses the capability of spectral feature extraction into GCN thus obtaining better superpixel representations than SPGCC, and improves the adjacency relationships between superpixels via evidence guided adaptive edge learning. As a result, our method outperforms SPGCC on all the four datasets.

Moreover, clustering map visualizations of different methods on *Indian Pines* and *Pavia University* are reported in Figs. 3 and 4. According to the visualizations, it is evident that our method demonstrates superior clustering for large-scale and continuously distributed land covers, e.g., dark green and dark yellow areas in *Indian Pines*, light green and light yellow areas in *Pavia University*. This advantage primarily stems from our method performing superpixel-level clustering and adopting the edge learning to construct a more accurate adjacency matrix for superpixels.

TABLE V
OPTIMAL HYPERPARAMETERS.

Dataset	M	L	α	β	γ
<i>Indian Pines</i>	275	2	0.5	0.01	0.45
<i>Pavia University</i>	1000	4	0.1	0.001	0.85
<i>Botswana</i>	4550	1	0.001	0.001	0.5
<i>Trento</i>	4400	2	0.005	0.1	0.7

D. Running Time Analysis

We report the running time of our method and other compared methods on four datasets in Table IV. In terms of the average running time, our method is only slower than SSC and SAPC, while faster than other eight methods, demonstrating that our method is lightweight and efficient. Compared to SSC, our method achieves significantly better clustering performance on all datasets. Compared to SAPC, our method demonstrates an improvement of over 10% in ACC on *Indian Pines* and *Botswana*, and an improvement of 4%-6% on other datasets. Therefore, the slight increase in running time is acceptable.

E. Hyperparameters Analysis

The proposed method mainly requires five hyperparameters: number of superpixels (M), number of network layers (L), weight of \mathcal{L}_{PC} (α), weight of \mathcal{L}_E (β) and momentum coefficient of edge weight updating (γ). We have tuned these hyperparameters for different datasets, and the adopted values are reported in Table V.

1) *Impact of M and L* : The number of superpixels (M) controls the segmentation of HSI and the homogeneity of superpixels, while the number of network layers (L) controls the margin of information aggregation and the receptive field of spectral feature convolution. For the proposed structural-spectral graph convolutional operator, one layer network enables superpixels to access their 1-hop neighbors. Large M with small L may lead to insufficient aggregation of spatial information in HSI, while small M with large L may result in over-smoothing representations of superpixels. As a result, according to Fig. 5, the optimal M on *Indian Pines*, *Pavia University*, *Botswana* and *Trento* are 275, 1000, 4550 and 4400, while the optimal L are 2, 4, 1 and 2 respectively.

2) *Impact of α and β* : α balances the influence between sample alignment and prototype contrast, while β controls whether the predicted edge weights are closer to the empirical edge weights or influenced by contrastive clustering. As shown in Fig. 6, our method is robust to α and β . We recommend selecting α and β from $\{0.01, 0.1\}$, as these values consistently yield promising clustering performance on different datasets.

3) *Impact of γ* : The momentum coefficient of edge weight updating (γ) determines the retention ratio of previous edge weights when updating the adjacency matrix. A smaller γ indicates a more aggressive update strategy. Generally, the proposed method is also robust to γ . According to Fig. 7, we suggest that γ could be set between [0.5, 0.8].

F. Further Analysis of Structural-Spectral Graph Convolutional Operator

To validate the effectiveness of the proposed structural-spectral graph convolutional operator (SSGCO), we compared it with a series of variant superpixel representation networks, including MLP, 1D-Conv, Graph-Conv, 1D-Graph-Conv and Graph-1D-Conv, as detailed below:

MLP: MLP that performs projection transformations is employed for superpixels.

1D-Conv: Several 1D convolutional layers are used to extract spectral features.

Graph-Conv: Several GCN layers are utilized to aggregate spatial information.

1D-Graph-Conv: Several 1D convolutional layers are applied to extract spectral features, followed by several GCN layers to aggregate spatial information.

Graph-1D-Conv: Several GCN layers are applied to aggregate spatial information, followed by several 1D convolutional layers to extract spectral features.

According to the experimental results presented in Table VI, the proposed SSGCO outperforms all other variant networks with a large margin. In addition, we have identified two observations.

First, compared to the MLP baseline, employing 1D-Conv alone improves the average ACC by 4.68% on four datasets, while employing Graph-Conv alone improves the average ACC by 7.11%. This demonstrates their capabilities of extracting high-order spectral features and aggregating spatial information. SSGCO integrates both spatial and spectral information of HSI effectively, thus leading to superior superpixel representations and clustering performance.

Second, comparing 1D-Graph-Conv, Graph-1D-Conv and SSGCO, both spectral feature extraction and spatial information aggregation are fused within each layer in SSGCO, while separated in 1D-Graph-Conv and Graph-1D-Conv. As a result, 1D-Graph-Conv and Graph-1D-Conv perform worse than SSGCO. Notably, Graph-1D-Conv yields the least favorable results. One possible reason is that several layers of projective transformations in GCN disrupt the continuity of spectral features, thereby limiting the effectiveness of subsequent 1D convolution.

G. Further Analysis of Evidence Guided Adaptive Edge Learning

In the proposed evidence guided adaptive edge learning (EGAEL) module, the predicted edge weight w^{pre} is generated by a learnable MLP based on current node representations and used to update the adjacency matrix. Differently, the empirical edge weight w^{emp} is calculated based on heuristic measures such as node similarity and clustering confidence. w^{emp} does not directly modify the graph, but instead serves as supervision to guide the learning of w^{pre} , encouraging w^{pre} to reflect more reliable inter-superpixel relationships.

To validate the effectiveness of w^{pre} and w^{emp} , we first conducted an ablation study. As shown in Table VII, the complete EGAEL module results in an average ACC improvement of 3.12%, while leveraging either w^{pre} or w^{emp} individually

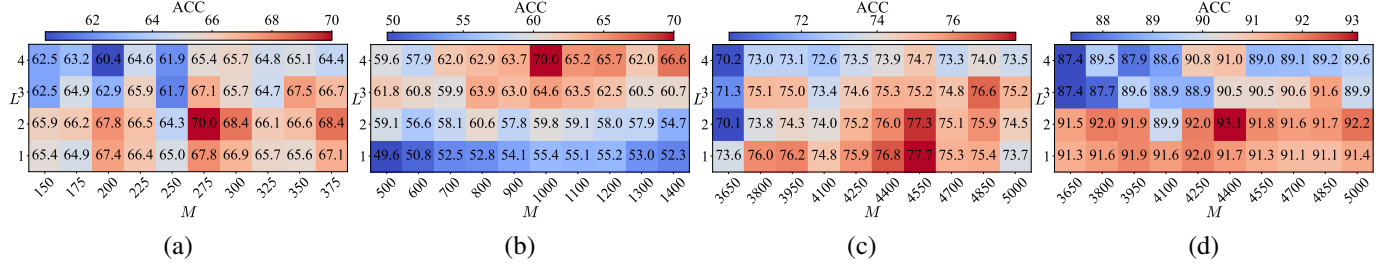


Fig. 5. The influence of different numbers of superpixels M and different numbers of network layers L on: (a) Indian Pines, (b) Pavia University, (c) Botswana and (d) Trento.

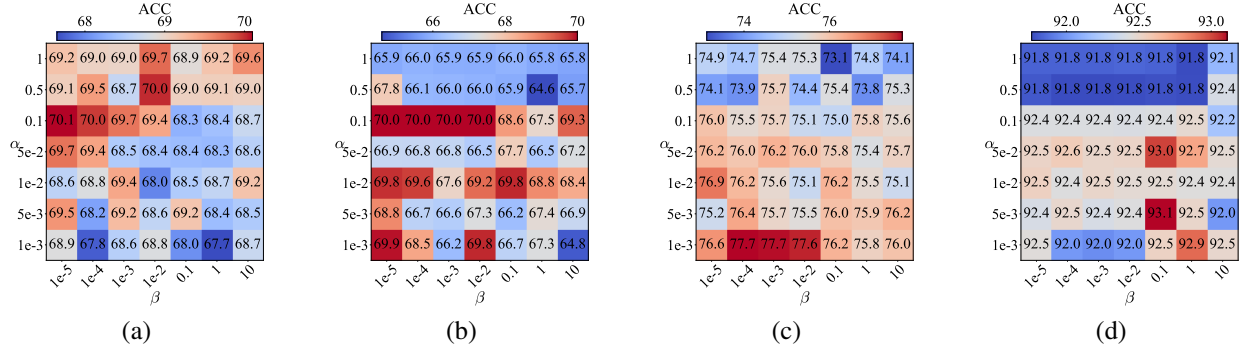


Fig. 6. The influence of different weights of \mathcal{L}_{PC} (α) and different weights of \mathcal{L}_E (β) on: (a) Indian Pines, (b) Pavia University, (c) Botswana and (d) Trento.

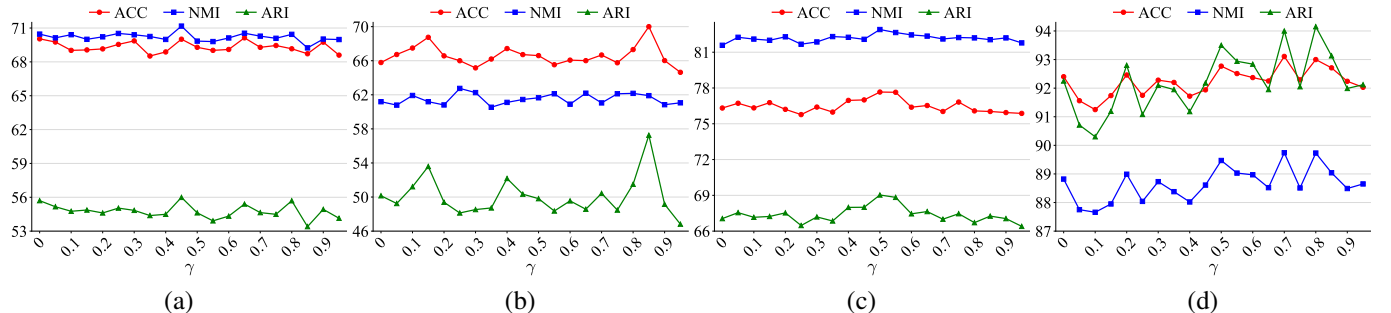


Fig. 7. The influence of different momentum coefficients of edge weight updating (γ) on: (a) Indian Pines, (b) Pavia University, (c) Botswana and (d) Trento.

yields inferior performance, underscoring the importance of their interaction within EGAEL module.

Next, we analyzed the value changes of w^{emp} during the training. We classified edges as correct or incorrect based on ground truth superpixel labels, which are determined by the majority class of internal labeled pixels. A correct edge connects two superpixels of the same class, otherwise, it is incorrect. We computed the average w^{emp} of correct and incorrect edges at each epoch, and conducted linear fitting, as shown in Fig. 8. On all datasets, the average w^{emp} of correct edges is consistently higher than that of incorrect edges. According to the fitted lines, correct edges exhibit significantly larger slope k than incorrect edges, indicating an increasing gap between correct and incorrect edges.

Then, we interpreted w^{pre} as the probability of an edge being correct, and determined an optimal threshold to classify correct and incorrect edges. The classification performance

is compared against that of using initial edge weights w^{init} , which assume all edges are correct. As shown in Table VIII, w^{pre} achieves higher accuracy on all the four datasets, with an improvement of 6.64% on Indian Pines dataset in particular. This demonstrates that the adjacency matrix constructed from w^{pre} is more reliable than the initial one, thereby validating the effectiveness of the proposed EGAEL module.

V. CONCLUSION

This paper presents a superpixel clustering method for HSI, centered on two key innovations: a structural-spectral graph convolutional operator (SSGCO) for enhanced HSI superpixel representation and an evidence guided adaptive edge learning (EGAEL) module for superpixel topological graph refinement. SSGCO infuses dedicated spectral convolution into the information aggregation of GNNs, enabling comprehensive extraction of both spatial and spectral information from superpixels. Complementarily, EGAEL adaptively optimizes the

TABLE VI
CLUSTERING PERFORMANCE OF VARIANT NETWORKS.

Network variations	Indian Pines			Pavia University			Botswana			Trento		
	ACC	NMI	ARI									
MLP	54.77 \pm 1.73	56.89 \pm 1.69	37.05 \pm 2.31	53.98 \pm 2.32	58.66 \pm 1.23	38.37 \pm 2.71	66.08 \pm 3.06	71.84 \pm 2.62	53.61 \pm 3.39	75.92 \pm 1.36	74.08 \pm 1.20	68.14 \pm 1.57
1D-Conv	56.54 \pm 0.68	58.16 \pm 0.92	37.98 \pm 0.62	60.88 \pm 3.01	65.31\pm2.85	47.12 \pm 6.27	74.37 \pm 4.53	79.03 \pm 1.83	63.91 \pm 4.73	77.66 \pm 3.58	71.89 \pm 2.88	66.52 \pm 4.17
Graph-Conv	64.31 \pm 0.70	66.47 \pm 0.72	48.67 \pm 1.65	56.62 \pm 2.69	47.23 \pm 2.15	40.53 \pm 6.57	71.03 \pm 2.13	75.65 \pm 2.05	59.31 \pm 3.06	87.24 \pm 4.08	81.85 \pm 3.04	84.40 \pm 5.83
1D-Graph-Conv	67.36 \pm 0.95	68.55 \pm 0.81	52.87 \pm 0.88	63.72 \pm 2.21	60.20 \pm 1.45	46.09 \pm 1.47	70.40 \pm 3.57	78.56 \pm 3.04	60.28 \pm 5.41	90.94 \pm 4.02	88.10 \pm 2.56	90.33 \pm 5.60
Graph-1D-Conv	62.18 \pm 3.33	65.90 \pm 1.69	46.22 \pm 2.88	51.73 \pm 5.83	46.59 \pm 5.26	36.44 \pm 8.49	66.08 \pm 2.53	74.79 \pm 1.58	55.69 \pm 1.34	92.06 \pm 0.97	87.01 \pm 0.45	92.49 \pm 0.83
SSGCO	70.01\pm1.95	71.17\pm1.31	55.99\pm2.07	70.00\pm3.46	61.90 \pm 3.18	57.26\pm8.57	77.66\pm1.28	82.90\pm1.30	69.03\pm2.38	93.11\pm0.96	89.74\pm0.94	94.00\pm1.30

TABLE VII
ABLATION STUDY RESULTS OF EVIDENCE GUIDED ADAPTIVE EDGE LEARNING.

w^{pre}	w^{emp}	Indian Pines			Pavia University			Botswana			Trento		
		ACC	NMI	ARI									
✓		67.45 \pm 1.43	68.07 \pm 1.42	53.13 \pm 1.04	64.96 \pm 1.40	60.54 \pm 4.22	46.20 \pm 4.27	74.06 \pm 0.82	81.78 \pm 0.92	66.89 \pm 1.23	91.85 \pm 1.08	88.63 \pm 1.25	92.68 \pm 2.13
✓	✓	69.54 \pm 1.90	70.02 \pm 1.30	54.79 \pm 2.91	68.26 \pm 3.36	62.66\pm3.44	54.64 \pm 7.43	76.64 \pm 1.97	82.32 \pm 0.92	67.93 \pm 2.28	92.40 \pm 1.53	89.05 \pm 1.42	92.86 \pm 2.51
✓	✓	67.86 \pm 0.72	68.88 \pm 1.05	52.81 \pm 1.23	64.88 \pm 1.78	62.36 \pm 1.54	47.71 \pm 1.82	73.39 \pm 2.14	81.10 \pm 1.14	65.50 \pm 1.75	90.90 \pm 1.46	87.68 \pm 1.49	90.99 \pm 2.94
		70.01\pm1.95	71.17\pm1.31	55.99\pm2.07	70.00\pm3.46	61.90 \pm 3.18	57.26\pm8.57	77.66\pm1.28	82.90\pm1.30	69.03\pm2.38	93.11\pm0.96	89.74\pm0.94	94.00\pm1.30

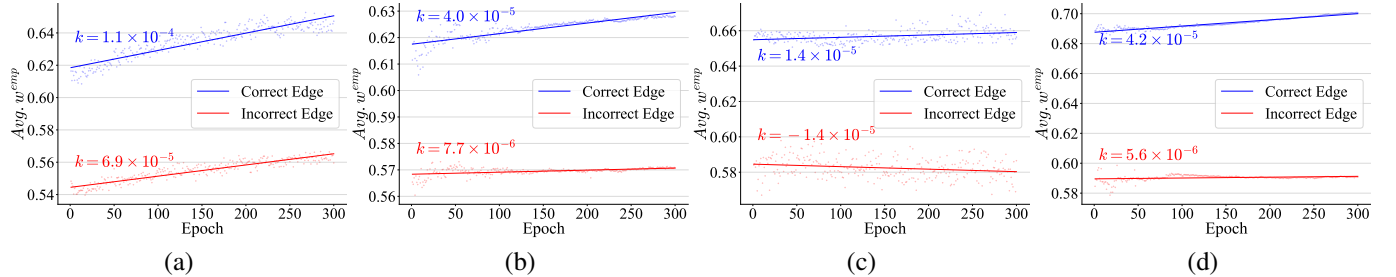


Fig. 8. Average empirical edge weight (w^{emp}) per epoch and the result of linear fitting on: (a) Indian Pines, (b) Pavia University, (c) Botswana and (d) Trento.

TABLE VIII
CLASSIFICATION ACCURACY (%) OF CORRECT AND INCORRECT EDGES WITH INITIAL EDGE WEIGHTS (w^{init}) AND PREDICTED EDGE WEIGHTS (w^{pre}).

Edge type	Indian Pines	Pavia University	Botswana	Trento
w^{init}	62.33	69.89	88.69	97.40
w^{pre}	68.97	73.54	90.59	97.64
Inc. \uparrow	6.64	3.65	1.90	0.24

superpixel topological graph by learning edge weights under the guidance of empirical edge weights, effectively mitigating the influence of initial incorrect connections. Finally, we integrate the proposed methods into a contrastive clustering framework, leveraging sample alignment and prototype contrast as clustering-oriented training objectives to achieve clustering. Extensive experiments on several HSI datasets demonstrate the effectiveness and superiority of our method.

REFERENCES

- [1] H. Liu, Y. Jia, J. Hou, and Q. Zhang, "Global-local balanced low-rank approximation of hyperspectral images for classification," *IEEE Trans. Circuits Syst. Video Technol.*, vol. 32, no. 4, pp. 2013–2024, 2022.
- [2] K. Chen, B. Chen, C. Liu, W. Li, Z. Zou, and Z. Shi, "Rsmamba: Remote sensing image classification with state space model," *IEEE Geosci. Remote Sens. Lett.*, vol. 21, pp. 1–5, 2024.
- [3] D. Hong, L. Gao, J. Yao, B. Zhang, A. Plaza, and J. Chanussot, "Graph convolutional networks for hyperspectral image classification," *IEEE Trans. Geosci. Remote Sens.*, vol. 59, no. 7, pp. 5966–5978, 2021.
- [4] J. Chen, K. Chen, H. Chen, W. Li, Z. Zou, and Z. Shi, "Contrastive learning for fine-grained ship classification in remote sensing images," *IEEE Trans. Geosci. Remote Sens.*, vol. 60, pp. 1–16, 2022.
- [5] D. Hong, Z. Han, J. Yao, L. Gao, B. Zhang, A. Plaza, and J. Chanussot, "Spectralformer: Rethinking hyperspectral image classification with transformers," *IEEE Trans. Geosci. Remote Sens.*, vol. 60, pp. 1–15, 2022.
- [6] F. Tian, S. Lei, Y. Zhou, J. Cheng, G. Liang, Z. Zou, H.-C. Li, and Z. Shi, "Hirennet: Hierarchical-relation network for few-shot remote sensing image scene classification," *IEEE Trans. Geosci. Remote Sens.*, vol. 62, pp. 1–10, 2024.
- [7] B. G. Ram, P. Oduor, C. Igathinathane, K. Howatt, and X. Sun, "A systematic review of hyperspectral imaging in precision agriculture: Analysis of its current state and future prospects," *Comput. Electron. Agric.*, vol. 222, p. 109037, 2024.
- [8] Y. Tang, S. Song, S. Gui, W. Chao, C. Cheng, and R. Qin, "Active and low-cost hyperspectral imaging for the spectral analysis of a low-light environment," *Sensors*, vol. 23, no. 3, 2023.
- [9] S. Hajaj, A. El Harti, A. B. Pour, A. Jellouli, Z. Adiri, and M. Hashim, "A review on hyperspectral imagery application for lithological mapping and mineral prospecting: Machine learning techniques and future prospects," *Remote Sens. Appl.: Soc. Environ.*, vol. 35, p. 101218, 2024.
- [10] X. Ma, Q. Man, X. Yang, P. Dong, Z. Yang, J. Wu, and C. Liu, "Urban feature extraction within a complex urban area with an improved 3d-cnn using airborne hyperspectral data," *Remote Sens.*, vol. 15, no. 4, 2023.
- [11] A. Kuras, M. Brell, J. Rizzi, and I. Burud, "Hyperspectral and lidar data applied to the urban land cover machine learning and neural-network-based classification: A review," *Remote Sens.*, vol. 13, no. 17, 2021.
- [12] N. A and A. A., "Current advances in hyperspectral remote sensing in urban planning," in *Proc. Int. Conf. Intell. Comput. Instrum. Control Technol. (ICICICT)*, 2022, pp. 94–98.
- [13] T. Kanungo, D. Mount, N. Netanyahu, C. Piatko, R. Silverman, and A. Wu, "An efficient k-means clustering algorithm: analysis and implementation," *IEEE Trans. Pattern Anal. Mach. Intell.*, vol. 24, no. 7, pp. 881–892, 2002.
- [14] T.-n. Yang, C.-j. Lee, and S.-j. Yen, "Fuzzy objective functions for robust

pattern recognition,” in *Proc. IEEE Int. Conf. Fuzzy Syst. (FUZZ-IEEE)*, 2009, pp. 2057–2062.

[15] E. Elhamifar and R. Vidal, “Sparse subspace clustering: Algorithm, theory, and applications,” *IEEE Trans. Pattern Anal. Mach. Intell.*, vol. 35, no. 11, pp. 2765–2781, 2013.

[16] R. Vidal and P. Favaro, “Low rank subspace clustering (lrsc),” *Pattern Recognit. Lett.*, vol. 43, pp. 47–61, 2014.

[17] R. A. Borsoi, T. Imbiriba, J. C. M. Bermudez, C. Richard, J. Chanussot, L. Drumetz, J.-Y. Tourneret, A. Zare, and C. Jutten, “Spectral variability in hyperspectral data unmixing: A comprehensive review,” *IEEE Geosci. Remote Sens. Mag.*, vol. 9, no. 4, pp. 223–270, 2021.

[18] J. Xie, R. Girshick, and A. Farhadi, “Unsupervised deep embedding for clustering analysis,” in *Proc. Int. Conf. Mach. Learn. (ICML)*, 2016, p. 478–487.

[19] R. Guan, Z. Li, X. Li, and C. Tang, “Pixel-superpixel contrastive learning and pseudo-label correction for hyperspectral image clustering,” in *Proc. IEEE Int. Conf. Acoust., Speech, Signal Process. (ICASSP)*, 2024, pp. 6795–6799.

[20] A. Yang, M. Li, Y. Ding, X. Xiao, and Y. He, “An efficient and lightweight spectral-spatial feature graph contrastive learning framework for hyperspectral image clustering,” *IEEE Trans. Geosci. Remote Sens.*, vol. 62, pp. 1–14, 2024.

[21] M.-Y. Liu, O. Tuzel, S. Ramalingam, and R. Chellappa, “Entropy rate superpixel segmentation,” in *Proc. IEEE/CVF Conf. Comput. Vis. Pattern Recognit. (CVPR)*, 2011, pp. 2097–2104.

[22] R. Achanta, A. Shajii, K. Smith, A. Lucchi, P. Fua, and S. Süsstrunk, “Slic superpixels compared to state-of-the-art superpixel methods,” *IEEE Trans. Pattern Anal. Mach. Intell.*, vol. 34, no. 11, pp. 2274–2282, 2012.

[23] Z. Li and J. Chen, “Superpixel segmentation using linear spectral clustering,” in *Proc. IEEE/CVF Conf. Comput. Vis. Pattern Recognit. (CVPR)*, 2015, pp. 1356–1363.

[24] X. Chen, Y. Zhang, X. Feng, X. Jiang, and Z. Cai, “Spectral-spatial superpixel anchor graph-based clustering for hyperspectral imagery,” *IEEE Geosci. Remote Sens. Lett.*, vol. 20, pp. 1–5, 2023.

[25] Z. Yuan and L. Yang, “Hyperspectral image clustering by superpixel-based low-rank constrained bipartite graph learning,” *IEEE Geosci. Remote Sens. Lett.*, vol. 21, pp. 1–5, 2024.

[26] Y. Ding, Z. Zhang, W. Kang, A. Yang, J. Zhao, J. Feng, D. Hong, and Q. Zheng, “Adaptive homophily clustering: Structure homophily graph learning with adaptive filter for hyperspectral image,” *IEEE Trans. Geosci. Remote Sens.*, vol. 63, pp. 1–13, 2025.

[27] H. Zhao, F. Zhou, L. Bruzzone, R. Guan, and C. Yang, “Superpixel-level global and local similarity graph-based clustering for large hyperspectral images,” *IEEE Trans. Geosci. Remote Sens.*, vol. 60, pp. 1–16, 2022.

[28] Y. Cai, Z. Zhang, P. Ghamisi, Y. Ding, X. Liu, Z. Cai, and R. Gloaguen, “Superpixel contracted neighborhood contrastive subspace clustering network for hyperspectral images,” *IEEE Trans. Geosci. Remote Sens.*, vol. 60, pp. 1–13, 2022.

[29] T. N. Kipf and M. Welling, “Semi-supervised classification with graph convolutional networks,” in *Proc. Int. Conf. Learn. Represent. (ICLR)*, 2017.

[30] P. Veličković, G. Cucurull, A. Casanova, A. Romero, P. Liò, and Y. Bengio, “Graph attention networks,” in *Proc. Int. Conf. Learn. Represent. (ICLR)*, 2018.

[31] Z. Wu, P. Jain, M. A. Wright, A. Mirhoseini, J. E. Gonzalez, and I. Stoica, “Representing long-range context for graph neural networks with global attention,” in *Proc. Int. Conf. Neural Inf. Process. Syst. (NIPS)*, ser. NIPS ’21, 2021.

[32] T. N. Kipf and M. Welling, “Variational graph auto-encoders,” in *Proc. Int. Conf. Neural Inf. Process. Syst. (NIPS)*, 2016.

[33] Y. Ding, Z. Zhang, X. Zhao, Y. Cai, S. Li, B. Deng, and W. Cai, “Self-supervised locality preserving low-pass graph convolutional embedding for large-scale hyperspectral image clustering,” *IEEE Trans. Geosci. Remote Sens.*, vol. 60, pp. 1–16, 2022.

[34] Y. Ding, Z. Zhang, X. Zhao, W. Cai, N. Yang, H. Hu, X. Huang, Y. Cao, and W. Cai, “Unsupervised self-correlated learning smoothly enhanced locality preserving graph convolution embedding clustering for hyperspectral images,” *IEEE Trans. Geosci. Remote Sens.*, vol. 60, pp. 1–16, 2022.

[35] F. Luo, Y. Liu, Y. Duan, T. Guo, L. Zhang, and B. Du, “Sdst: Self-supervised double-structure transformer for hyperspectral images clustering,” *IEEE Trans. Geosci. Remote Sens.*, vol. 62, pp. 1–14, 2024.

[36] Y. Zhang, Y. Wang, X. Chen, X. Jiang, and Y. Zhou, “Spectral-spatial feature extraction with dual graph autoencoder for hyperspectral image clustering,” *IEEE Trans. Circuits Syst. Video Technol.*, vol. 32, no. 12, pp. 8500–8511, 2022.

[37] J. Chen, S. Liu, and H. Wang, “Dual smooth graph convolutional clustering for large-scale hyperspectral images,” *IEEE J. Sel. Top. Appl. Earth Obs. Remote Sens.*, vol. 17, pp. 6825–6840, 2024.

[38] K. He, H. Fan, Y. Wu, S. Xie, and R. Girshick, “Momentum contrast for unsupervised visual representation learning,” in *Proc. IEEE/CVF Conf. Comput. Vis. Pattern Recognit. (CVPR)*, 2020, pp. 9726–9735.

[39] J.-B. Grill, F. Strub, F. Altché, C. Tallec, P. H. Richemond, E. Buchatskaya, C. Doersch, B. A. Pires, Z. D. Guo, M. G. Azar, B. Piot, K. Kavukcuoglu, R. Munos, and M. Valko, “Bootstrap your own latent: A new approach to self-supervised learning,” in *Proc. Int. Conf. Neural Inf. Process. Syst. (NIPS)*, 2020.

[40] Z. Huang, J. Chen, J. Zhang, and H. Shan, “Learning representation for clustering via prototype scattering and positive sampling,” *IEEE Trans. Pattern Anal. Mach. Intell.*, vol. 45, no. 6, pp. 7509–7524, 2023.

[41] J. Qi, Y. Jia, H. Liu, and J. Hou, “Superpixel graph contrastive clustering with semantic-invariant augmentations for hyperspectral images,” *IEEE Trans. Circuits Syst. Video Technol.*, vol. 34, no. 11, pp. 11360–11372, 2024.

[42] H. Zhai, H. Zhang, P. Li, and L. Zhang, “Hyperspectral image clustering: Current achievements and future lines,” *IEEE Geosci. Remote Sens. Mag.*, vol. 9, no. 4, pp. 35–67, 2021.

[43] A. van den Oord, Y. Li, and O. Vinyals, “Representation learning with contrastive predictive coding,” *arXiv:1807.03748*, 2019.

[44] S. Ioffe and C. Szegedy, “Batch normalization: accelerating deep network training by reducing internal covariate shift,” in *Proc. Int. Conf. Mach. Learn. (ICML)*, 2015, pp. 448–456.

[45] P. Lu, X. Jiang, Y. Zhang, X. Liu, Z. Cai, J. Jiang, and A. Plaza, “Spectral-spatial and superpixelwise unsupervised linear discriminant analysis for feature extraction and classification of hyperspectral images,” *IEEE Trans. Geosci. Remote Sens.*, vol. 61, pp. 1–15, 2023.

[46] K. Cui, R. Li, S. L. Polk, Y. Lin, H. Zhang, J. M. Murphy, R. J. Plemmons, and R. H. Chan, “Superpixel-based and spatially regularized diffusion learning for unsupervised hyperspectral image clustering,” *IEEE Trans. Geosci. Remote Sens.*, vol. 62, pp. 1–18, 2024.

[47] G. Jiang, Y. Zhang, X. Wang, X. Jiang, and L. Zhang, “Structured anchor learning for large-scale hyperspectral image projected clustering,” *IEEE Trans. Circuits Syst. Video Technol.*, vol. 35, no. 3, pp. 2328–2340, 2025.

[48] H. W. Kuhn, “The hungarian method for the assignment problem,” *Nav. Res. Logist.*, vol. 2, no. 1-2, pp. 83–97, 1955.



Jianhan Qi received the B.S. degree in Computer Science and Technology from Wuhan University of Technology, Wuhan, China in 2022. He is currently working toward the M.S. degree in Software Engineering from Southeast University, Nanjing, China. His research interests include unsupervised learning and graph neural networks.



Yuheng Jia (Member, IEEE) received the B.S. degree in automation and the M.S. degree in control theory and engineering from Zhengzhou University, Zhengzhou, China, in 2012 and 2015, respectively, and the Ph.D. degree in computer science from the City University of Hong Kong, Hong Kong, China, in 2019. He is currently an Associate Professor with the School of Computer Science and Engineering, Southeast University, Nanjing, China. His research interests include machine learning and data representation, such as un/semi/weakly-supervised learning, modeling and analysis, and low-rank tensor/matrix approximation and factorization.

high-dimensional data modeling and analysis, and low-rank tensor/matrix approximation and factorization.



Hui Liu received the B.Sc. degree in communication engineering from Central South University, Changsha, China, the M.Eng. degree in computer science from Nanyang Technological University, Singapore, and the Ph.D. degree in computer science from the City University of Hong Kong, Hong Kong, China. From 2014 to 2017, she was a Research Associate with the Maritime Institute, Nanyang Technological University. She is currently an Assistant Professor with the School of Computing Information Sciences, Caritas Institute of Higher Education, Hong Kong, China. Her current research interests include image processing and machine learning.



Junhui Hou (Senior Member, IEEE) is an Associate Professor with the Department of Computer Science, City University of Hong Kong. He holds a B.Eng. degree in information engineering (Talented Students Program) from the South China University of Technology, Guangzhou, China (2009), an M.Eng. degree in signal and information processing from Northwestern Polytechnical University, Xi'an, China (2012), and a Ph.D. degree from the School of Electrical and Electronic Engineering, Nanyang Technological University, Singapore (2016). His research interests are multi-dimensional visual computing. Dr. Hou received the Early Career Award (3/381) from the Hong Kong Research Grants Council in 2018 and the NSFC Excellent Young Scientists Fund in 2024. He has served or is serving as an Associate Editor for IEEE Transactions on Visualization and Computer Graphics, IEEE Transactions on Image Processing, IEEE Transactions on Multimedia, and IEEE Transactions on Circuits and Systems for Video Technology.